Environmental Science and Pollution Research (2019) 26:7772–7784
https://doi.org/10.1007/s11356-018-4019-2

RESEARCH ARTICLE

A comparative study on the photo-catalytic degradation of Cytarabine anticancer drug under Fe^{3+}/H_2O_2, $Fe^{3+}/S_2O_8^{2-}$, and $[Fe(C_2O_4)_3]^{3-}/H_2O_2$ processes. Kinetics, identification, and in silico toxicity assessment of generated transformation products

Anastasia Koltsakidou[1] · Maria Antonopoulou[2] · Eleni Evgenidou[1] · Ioannis Konstantinou[3] · Dimitra Lambropoulou[1]

Received: 5 June 2018 / Accepted: 17 December 2018 / Published online: 23 January 2019

Abstract

Cytarabine (CY) is an anticancer drug which has been identified in wastewater influents, effluents, and surface waters. In the present study, the degradation of CY under simulated solar light (SSL), by photo-Fenton (Fe^{3+}/H_2O_2/SSL) and photo-Fenton-like processes ($Fe^{3+}/S_2O_8^{2-}$/SSL and $[Fe(C_2O_4)_3]^{3-}/H_2O_2$/SSL), was investigated. The major parameters affecting the applied treatments (e.g., concentration of CY, Fe^{3+}, H_2O_2, and $S_2O_8^{2-}$) were optimized and CY's complete removal was achieved within 45 min for all techniques used. Mineralization studies indicated that $[Fe(C_2O_4)_3]^{3-}/H_2O_2$/SSL treatment was the most efficient procedure since faster kinetics are achieved and higher mineralization percentage is reached compared to the other techniques used. Furthermore, 12 transformation products (TPs) were identified during the applied processes, by high resolution mass spectrometry, four of which were identified for the first time, indicating that CY molecule undergoes hydroxylation and subsequent oxidation, during the applied processes. Moreover, predictions of acute and chronic ecotoxicity of CY and its TPs on fish, daphnia, and green algae were conducted, using in silico quantitative structure activity relationship (QSAR) calculations. According to these predictions, the TPs generated during the studied treatments may pose a threat to aquatic environment. Finally, the efficiency of CY degradation by photo-Fenton and photo-Fenton-like treatment in real wastewater was evaluated, under the optimized conditions, which resulted in lower degradation rate constants compared to ultrapure water.

Keywords Cytarabine · In silico assessment of toxicity · Solar photo-Fenton · Transformation products

Introduction

Cytarabine (CY) is an antimetabolite, used as an anticancer drug for lymphoma and acute leukemia. It is also used as an antiviral agent against herpes simplex virus and human cytomegalovirus (Liu et al. 2014). Similar to all drugs, CY is excreted through feces and urine, after administrated to patients, as mixture of unchanged parent compound and its metabolites. This mixture enters the aquatic environment through hospital and municipal wastewaters (Isidori et al. 2016a). Its urinary excretion rate is ~ 10% and its half-life degradation in the human body is 1–3 h (Zhang et al. 2013). As a result, CY has been found in concentrations up to 9.2, 14, and 13 ng L^{-1} in wastewater (influents and effluents) and surface water, respectively (Kosjek and Heath 2011, Martín et al. 2011). The presence of anti-cancer drugs, like CY, in effluents indicates limited removal in wastewater treatment plants (Isidori et al. 2016b). Additionally, potential toxic effects in organisms exposed to continuous or intermittent presence of parent anticancer drugs and their transformation products (TPs) cannot be ignored (Toolaram et al. 2014). Under this light, the development of effective alternative processes for wastewater treatment is

Responsible editor: Vítor Pais Vilar

Electronic supplementary material The online version of this article (https://doi.org/10.1007/s11356-018-4019-2) contains supplementary material, which is available to authorized users.

✉ Dimitra Lambropoulou
dlambro@chem.auth.gr

[1] Department of Chemistry, Aristotle University of Thessaloniki, 54124 Thessaloniki, Greece

[2] Department of Environmental and Natural Resources Management, University of Patras, 30100 Agrinio, Greece

[3] Department of Chemistry, University of Ioannina, 45110 Ioannina, Greece

necessary, in order to prevent the entrance of these compounds to the aquatic environment.

A promising approach for the removal of pharmaceuticals, such as anti-cancer drugs, that gained recognition is advanced oxidation processes (AOPs) (Koltsakidou et al. 2017c, Lin and Lin 2014, Lutterbeck et al. 2015a, b). The degradation of recalcitrant pollutants by AOPs is resulting from the formation of highly reactive hydroxyl radicals ($HO^{\cdot}$). $HO^{\cdot}$ can lead to total mineralization of a variety of organic compounds (Ribeiro et al. 2015). CY degradation has been studied by several AOPs so far, including TiO_2 photocatalysis, ozonation, UV/H_2O_2, UV/$K_2S_2O_8$, and other radical promoter systems, gamma radiation, and TiO_2/activated carbon under UV radiation (Koltsakidou et al. 2017a, Ocampo-Pérez et al. 2010, 2011, 2016). Although some of these treatments are very effective in CY degradation, they suffer from some major disadvantages. For example, ozonation may result in the formation of the potentially toxic oxidation by-product bromate in bromide-containing wastewaters (Soltermann et al. 2017). Additionally, ozone has an extremely short half-life for only 20 min and low solubility in water. As far as TiO_2 heterogeneous photocatalysis is concerned, post-treatment recovery of the catalyst particles after water treatment is required while inefficient exploitation of visible light hinders its use (Dong et al. 2015). On the other hand, UV irradiation has limited treatment times, suffers from light-screening water constituents while leading to energy depletion and high operational costs for complete destruction (Katheresan et al. 2018). Furthermore, recent investigations are concentrated on methods that can exploit more efficiently solar light for reducing considerably operating costs. The photo-Fenton process has gained increasing attention due to its simplicity and the possibility of using sunlight for its application.

Since the generation of intermediates is inevitable during AOPs application, the determination of their chemical structure and toxicity is crucial. In silico methods (methods based on computer simulation) for the prediction of toxicity have been increasingly used by researchers during the last decade (Raies and Bajic 2016). ECOSAR is a computer program, developed by EPA, that estimates the toxicity of chemicals to aquatic organisms, such as fish (both in fresh and saltwater), invertebrates, and algae, without test data. ECOSAR's calculations are based on structure–activity relationships (SARs) for the prediction of chemicals' aquatic toxicity, depending on the similarity of their molecular structures to other compounds for which the aquatic toxicity is known.

So far, no efforts have been done to study the photocatalytic degradation of CY compound using photo-Fenton and photo-Fenton-like processes under simulated solar light (SSL), as well as to predict the ecotoxicity of CY and its TPs by applying in silico prediction tools using QSAR models, to the best of our knowledge. In addition, CY intermediates described in the literature have been determined using LC-MS techniques (Koltsakidou et al. 2017a), which do not allow MS^n fragmentation and therefore their identification is still not fully explored.

Considering the above-mentioned issues and the scarcity of studies evaluating the degradation of CY by photo Fenton processes, the main objectives of this study were as follows: (1) to obtain new information on the treatment and transformation of CY by using photo-Fenton and photo-Fenton-like approaches under simulated solar irradiation, (2) to estimate the removal and mineralization effectiveness and suitability of different solar treatments, (3) to provide comprehensive insight concerning the formation and elucidation of TPs by using Orbitrap-LC/MS/MS, and (4) to apply in silico methods at various toxicological endpoints for the assessment of toxicity of TPs.

Experimental

Reagents and materials

The studied anti-cancer drug CY (> 98%) was purchased from TCI (Tokyo Chemical Industry Co.). The HPLC–MS grade organic solvents (methanol and acetonitrile) used for chromatographic analysis were supplied by Merck (Darmstadt, Germany). The salts used for ion chromatography analyses (Na_2CO_3 and $NaHCO_3$) were purchased from Sigma–Aldrich (Germany). Hydrogen peroxide (H_2O_2, 30% *w*/*v*) was obtained from Panreac (Barcelona, Spain). All the salts used for the oxidation techniques ($FeCl_3{\cdot}6H_2O$, $C_2K_2O_4{\cdot}1H_2O$, $Na_2S_2O_8$ > 99 + %) were supplied from Chem-Lab NV (Zedelgem, Belgium). The water used for chromatographic analysis and photocatalytic experiments was ultrapure water (Millipore Waters Milli-Q water purification system).

Photodegradation experiments

The equipment used in the study as well as the experimental conditions for the photo-Fenton experiments has been reported in detail previously (Koltsakidou et al. 2017b). Briefly, the simulated solar irradiation was conducted by Atlas Suntest CPS+ (Germany), which was equipped with a xenon lamp (< 290 nm) with a constant irradiance of 500 Wm^{-2}. CY solutions (10 mg L^{-1}) were acidified (pH 2.9–3), before each experiment, using HCl, in order to prevent iron precipitation. Measurements of pH at various irradiation times and at the end of the treatment show no significant variation from the starting values. For the determination of mineralization's evolution, as well as the identification of TPs, 30 mg L^{-1} of CY was used as initial concentration, in order to obtain

slower kinetics and facilitate their detection. Ferrioxalate was also prepared as reported in previous studies (Doumic et al. 2015, Monteagudo et al. 2010).

Analytical procedures

CY determination

CY concentration, during the photodegradation experiments, was determined by an HPLC system with SPD 20A DAD detector coupled in series with the LC–MS 2010EV mass selective detector obtained from Shimadzu (Kyoto, Japan). The exact conditions of CY determination have been reported in a previous work (Koltsakidou et al. 2017a).

Mineralization studies

A Shimadzu TOC V-csh Analyzer was used for the determination of total organic carbon (TOC) concentration. NO_3^- ions were quantified by an ion chromatography (Metrohm) as reported in a previous study (Koltsakidou et al. 2017a).

By-product evaluation

The intermediates formed during CY photodegradation were characterized by an LTQ Orbitrap Discovery MS high resolution system that operated in positive ionization mode. The chromatographic analysis was conducted using an Acquity UPLC HSS T3 column (100 × 2.1 mm, 1.8 μm, Waters, Milford, MA, USA), at a constant temperature of 40 °C and a flow rate of 500 L min^{-1}. The mobile phases used were water/formic acid (0.1% *v*/*v*) (phase A) and methanol/formic acid (0.1% *v*/*v*) (phase B). The chromatographic separation was obtained by the application of a linear gradient (90% A to 0% A in 15 min, 90% A in 20 min). ESI source parameters were described in a previous work (Antonopoulou et al. 2013).

Ecotoxicity assessment

Predictions of ecotoxicity (acute and chronic) of CY and its TPs on fish, daphnia, and green algae were conducted by ECOlogical Structure-Activity Relationship Model (ECOSAR), a program (version 1.11) developed by USEPA (https://www.epa.gov/tsca-screening-tools/ecological-structure-activity-relationships-ecosar-predictive-model). The detailed description of ECOSAR predictions has been already reported elsewhere (Ferri et al. 2017).

Results and discussion

Optimization of photo-Fenton treatment

Preliminary Fe^{3+}/H_2O_2 and Fe^{3+}/H_2O_2/SSL degradation experiments

Experiments in the dark and under SSL by employing the Fe^{3+}/H_2O_2 system for the degradation of CY were conducted and compared as a preliminary study. Figure 1 summarizes the obtained results. Under no irradiation, only 10% reduction is achieved during the first 20 min. During the same period of time, the reduction achieved by Fe^{3+}/H_2O_2/SSL treatment is approximately 99%. The effect of simulated solar light irradiation alone is also depicted in Fig. 1. Obviously, photolysis provokes no significant degradation (20% after 60 min of irradiation) of CY, compared to Fe^{3+}/H_2O_2/SSL treatment. The above preliminary results indicate that photolysis as well as dark reaction (Fe^{3+}/H_2O_2) has minus contribution to the degradation of CY, when Fe^{3+}/H_2O_2/SSL treatment is applied.

Degradation kinetics and effect of initial CY concentration

Since the reaction between $HO^{\cdot}$ and CY is the rate-determining step, as reported to previous homogeneous photocatalytic studies for pollutants (Evgenidou et al. 2007, Martínez-Costa et al. 2018), the studied photo-Fenton process can be expressed by Eq. (1):

$$r = -\frac{dC}{dt} = k_{HO}[HO^{\cdot}]C \quad (1)$$

where *C* is the concentration of CY and k_{HO} is the reaction rate constant.

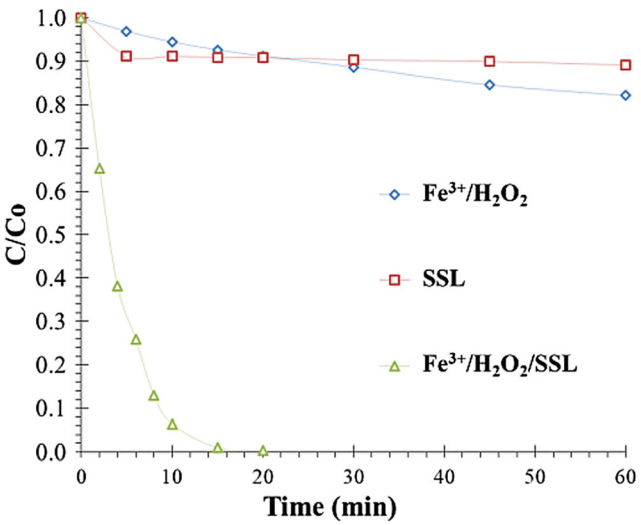

Fig. 1 Photo-Fenton treatment of CY in comparison to Fenton treatment and direct photolysis (experimental conditions: C_o(CY) = 10 mg L^{-1}, [Fe^{3+}] = 1 mg L^{-1}, [H_2O_2] = 30 mg L^{-1})

Because $HO^{\cdot}$ steady-state concentration is reached quite fast, the above equation can also be written as Eq. (2):

$$r = -\frac{dC}{dt} = k_{HO}[HO^{\cdot}]C = k_{app}C \quad (2)$$

where k_{app} is the apparent pseudo-first-order constant.

In this study, the above pseudo-first-order model appeared to fit well the experimental data ($R^2 > 0.995$ for $\ln(C_0/C)$ vs. time (t)), and the apparent k_{app} values were obtained by linear fitting from the degradation curves. For minimization of variations resulting from competitive effects of intermediates, only the data exported from the first minutes of irradiation were taken into consideration for the calculation of k_{app}.

For the evaluation of CY initial concentration influence to the reaction rate (k_{app}), experiments were carried out at various concentrations of CY, varying from 10 to 50 mg L^{-1}, while the concentration of Fe^{3+} and H_2O_2 were kept constant at 1 mg L^{-1} and 60 mg L^{-1}, respectively. As indicated in Fig. 2a, an increase in the initial concentration of CY till 50 mg L^{-1} leads to a decrease of the apparent rate constant, which later reaches a plateau. The effectiveness of photo-Fenton process depends highly on the formation of hydroxyl radicals and their ratio to the initial concentration of the substrate. Consequently, since the concentration of the target compound is increased and the initial concentration of the hydroxyl radicals remains the same, the degradation of the target compound will need longer irradiation times under identical experimental conditions (Michael et al. 2010). Moreover, higher substrate concentration may absorb a fraction of light decreasing the activation of the catalyst thus decreasing the formation of hydroxyl radicals (Lambropoulou et al. 2017, Tamimi et al. 2008).

Effect of iron concentration

Since iron residues in effluents and sludge are considered harmful to the environment, low concentrations (lower than 5 mg L^{-1}) that result in short reaction times, avoiding the need of further treatment for iron removal, are preferable (Gar Alalm et al. 2015). In this study, the effect of iron concentration was evaluated by the addition of 0–2.5 mg L^{-1} Fe^{3+}, 60 mg L^{-1} H_2O_2, and 10 mg L^{-1} initial concentration of CY. Figure 2b represents the evolution of degradation rate within the studied concentration levels of Fe^{3+}. The addition of Fe^{3+} increases the reaction rate in a linear trend which is attributed to the proportional amount of $HO^{\cdot}$ formation, as indicated by photo-Fenton reactions (Eq. 3):

$$Fe^{3+} + H_2O \xrightarrow{h\nu} HO^{\cdot} + Fe^{2+} + H^{+} \quad (3)$$

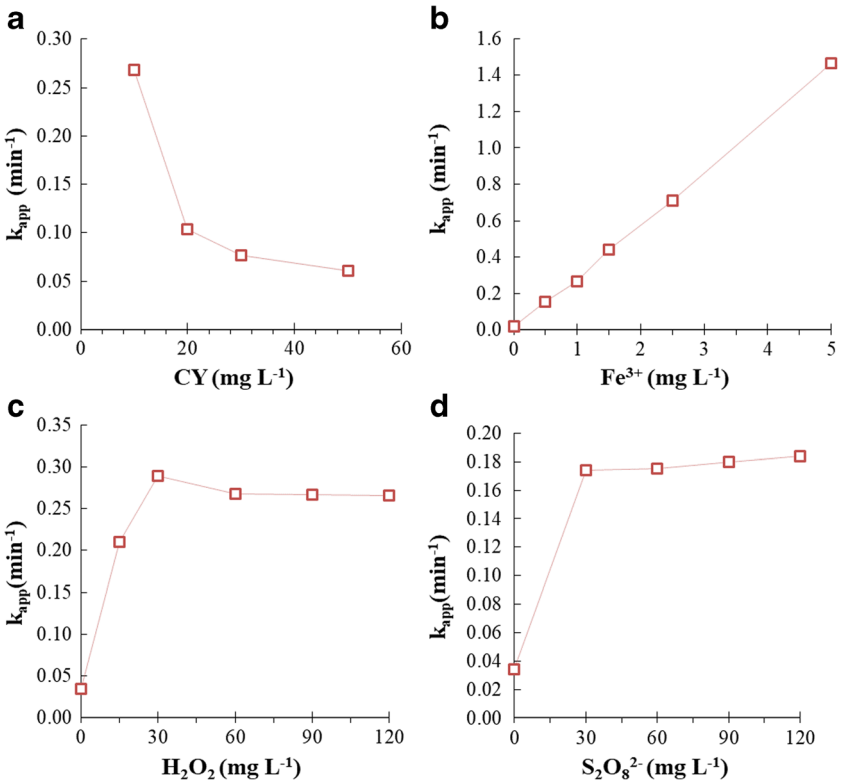

Fig. 2 The effect of operational parameters on CY photo-Fenton degradation; effect of CY loading ($[Fe^{3+}] = 1$ mg L^{-1}, $[H_2O_2] =$ 60 mg L^{-1}) (**a**); Effect of Fe^{3+} loading ($C_o(CY) = 10$ mg L^{-1}, $[H_2O_2] = 60$ mg L^{-1}) (**b**); Effect of H_2O_2 loading ($C_o(CY) =$ 10 mg L^{-1}, $[Fe^{3+}] = 1$ mg L^{-1}) (**c**); Effect of $S_2O_8^{2-}$ loading ($C_o(CY) = 10$ mg L^{-1}, $[Fe^{3+}] =$ 1 mg L^{-1}) (**d**)

Moreover, according to Eq. (3), ferric ions are photoreduced to ferrous ions which are the main species that catalyze hydrogen peroxide (Fenton reactions (Eqs. 4–6)) thus producing additional radicals such as $HO^{\cdot}$ and $HO_2^{\cdot}$.

$$Fe^{2+} + H_2O_2 \rightarrow Fe^{3+} + OH^- + HO^{\cdot} \quad (4)$$

$$Fe^{3+} + H_2O_2 \rightarrow Fe\text{–}OOH^{2+} + H^+ \quad (5)$$

$$Fe\text{–}OOH^{2+} \rightarrow HO_2^{\cdot} + Fe^{2+} \quad (6)$$

Additionally, when no Fe^{3+} are added, a low degradation of CY is still observed due to the photolysis of H_2O_2 under UV radiation (Irmak et al. 2004), as descripted by Eq. (7):

$$H_2O_2 \xrightarrow{h\nu} 2HO^{\cdot} \quad (\lambda < 320\ \text{nm}) \quad (7)$$

However, the overlap of the adsorption spectrum of hydrogen peroxide with the emission spectrum of xenon lamp of the solar simulator is very small; hence, a minor degradation rate was observed in the absence of iron.

All in all, for further experiments, the concentration of 1 mg L^{-1} was selected, since higher concentrations of Fe^{3+} would result in much faster degradation of CY, that disable the proper monitoring of the degradation kinetics.

Effect of H_2O_2 concentration

During photo-Fenton process, hydrogen peroxide's initial concentration is crucial for achieving effective oxidation of the organic substrate. The efficiency of the applied procedure may be decreased both by low and excess of H_2O_2 (Bautitz and Nogueira 2010). In this study, concentrations varying from 0 to 120 mg L^{-1} of H_2O_2 were examined. As indicated in Fig. 2c, the k_{app} increases till the concentration of 30 mg L^{-1}, reaching a plateau or even decrease a little thereafter. This decrease can be explained by the enhancement of parallel reactions, such as scavenging of generated $HO^{\cdot}$ by H_2O_2 as described below (Eqs. (8–10)) (Abdessalem et al. 2008, Dal Bosco et al. 2011).

$$H_2O_2 + HO^{\cdot} \rightarrow HO_2^{\cdot} + H_2O \quad (8)$$

$$2H_2O_2 \rightarrow 2H_2O + O_2 \quad (9)$$

$$2HO^{\cdot} \rightarrow H_2O + 1/2O_2 \quad (10)$$

Therefore, the concentration of 30 mg L^{-1} has been chosen for further experiments.

In addition, when no peroxide was added to the treated solution, photodegradation of the target compounds still occurs. This may be attributed to the excitation of the $[Fe^{III}OH(H_2O)_5]^{2+}$ complex which is the dominant specie in the aquatic solution of the target compound at pH ~ 3. This aqua-complex can produce also hydroxyl radicals under irradiation following Eq. (11):

$$\left[Fe^{III}OH(H_2O)_5\right]^{2+} + H_2O + h\nu \rightarrow \left[Fe^{II}(H_2O)_6\right]^{2+} + HO^{\cdot} \quad (11)$$

Moreover, photodegradation of CY in the absence of peroxide can also occur through the formation of Fe-CY complex since cytarabine disposes functional groups that can be acted as ligands to Fe(III). As reported elsewhere, Fe(III) complexes may exhibit higher absorbance and higher quantum yields than simple aquated Fe(III) species, and therefore may be more important in photo-Fenton systems (Pignatello et al. 2006). Méndez-Arriaga et al. (2010) (Méndez-Arriaga et al. 2010) showed that Fe(III) bounds with the organic target compound (ibuprofen) thus forming a complex that is photoactive. This complex promotes in a strong manner the decarboxylation of the organic substrate.

Comparison of photo-Fenton with persulfate and Fenton-like treatments of CY

The efficiency of Fe^{3+}/H_2O_2/SSL photocatalytic system was compared with $Fe^{3+}/S_2O_8^{2-}$/SSL and $[Fe(C_2O_4)_3]^{3-}/H_2O_2$/SSL systems, regarding the reaction rate and the mineralization percentage achieved in each case.

Sulfate radicals ($SO_4^{\cdot-}$, $E_0 = 2.60$ V), which can be produced by activation of peroxodisulphate, are an alternative oxidant that has been lately studied as degradation agent for several organic pollutants (Ding et al. 2017, Ismail et al. 2017, Soltani and Lee 2017). Also, sulfate radicals present a longer life-time than hydroxyl radicals (Gao et al. 2016) and are more selective towards organic substrates reacting via direct electron transfer mechanism (Kamińska et al. 2018, Matta et al. 2011). In this study, $SO_4^{\cdot-}$ is produced by the reaction of peroxodisulphate and Fe(III) as described in Eqs. (12) and (13) (Avetta et al. 2015, Hu et al. 2016):

$$Fe(III) + S_2O_8^{2-} \rightarrow Fe(II) + S_2O_8^{\cdot-} \quad (12)$$

$$Fe(II) + S_2O_8^{2-} \rightarrow Fe(III) + SO_4^{2-} + SO_4^{\cdot-} \quad (13)$$

The studied concentrations of added peroxodisulphate in this study were 0–120 mg L^{-1}, while the concentration of Fe (III) was 1 mg L^{-1} for comparison purposes with the Fe^{3+}/H_2O_2 process. As indicated in Fig. 2d, the degradation rate of CY is almost fivefold increased by the addition of

peroxodisulphate up to 30 mg L^{-1}, while a near plateau is observed for higher concentration levels. As a result, the concentration level of 30 mg L^{-1} is considered the most suitable under the current experimental conditions.

Ferrioxalate system has been also considered as an efficient alternative to Fe^{3+}/H_2O_2 system for the degradation of pollutants, since it can expand the usage of solar spectrum range up to 450 nm, improving the solar-Fenton process (Li et al. 2015). Furthermore, the photolysis of ferrioxalate complex leads to additional oxidants according to the following equations (Lucas and Peres 2007):

$$\left[Fe(C_2O_4)_3\right]^{3-} \xrightarrow{h\nu} Fe(II) + 2C_2O_4^{2-} + C_2O_4^{\cdot-} \quad (14)$$

$$C_2O_4^{\cdot-} + \left[Fe(C_2O_4)_3\right]^{3-} \rightarrow Fe(II) + 3C_2O_4^{2-} + 2CO_2 \quad (15)$$

$$C_2O_4^{\cdot-} + O_2 \rightarrow O_2^{\cdot-} + 2CO_2 \quad (16)$$

In order to compare the three homogeneous photocatalytic treatments of CY, by means of mineralization as well as to identify and compare the TPs generated by each procedure, three times higher initial concentration of CY was selected (30 mg L^{-1}), which enables simpler and less laborious procedures for the monitoring of their evolution. The concentration of ferric ions and the concentration of the oxidant were also increased three times (3 mg L^{-1} and 90 mg L^{-1} in each case), so that the reaction kinetics are close to those obtained by the previous experiments. Under the selected experimental conditions, the reaction rates were 0.353, 0.162, and 0.379 min^{-1} for Fe^{3+}/H_2O_2/SSL, $Fe^{3+}/S_2O_8^{2-}$/SSL, and $[Fe(C_2O_4)_3]^{3-}/H_2O_2$/SSL respectively. The addition of oxalate enhances TOC reduction of CY solution, as indicated in Fig. 3. The TOC reduction achieved by Fe^{3+}/H_2O_2/SSL and $Fe^{3+}/S_2O_8^{2-}$/SSL treatments is approximately 73%, while TOC reduction reaches 82% by $[Fe(C_2O_4)_3]^{3-}/H_2O_2$/SSL treatment, after 360 min of SSL irradiation. On the other hand, no significant difference is observed at all three treatments, as far as NO_3^- release is concerned, which was quite low (3–4% in all cases), indicating the formation of TPs that preserves N atoms. Consequently, it appears that $[Fe(C_2O_4)_3]^{3-}/H_2O_2$/SSL treatment is the most efficient among the studied processes. This result is in agreement with previous studies since it has been proven that counter ion of iron can play important role in the photodegradation kinetics (Evgenidou et al. 2007). More specifically, anions in general, that may originate either from background electrolytes or Fe^{3+} counter ion or even H^+ counter ion, can affect the photocatalysed degradation of the target compound. Oxalates appear to give higher reaction rates since chloride ions may create complexes with iron thus

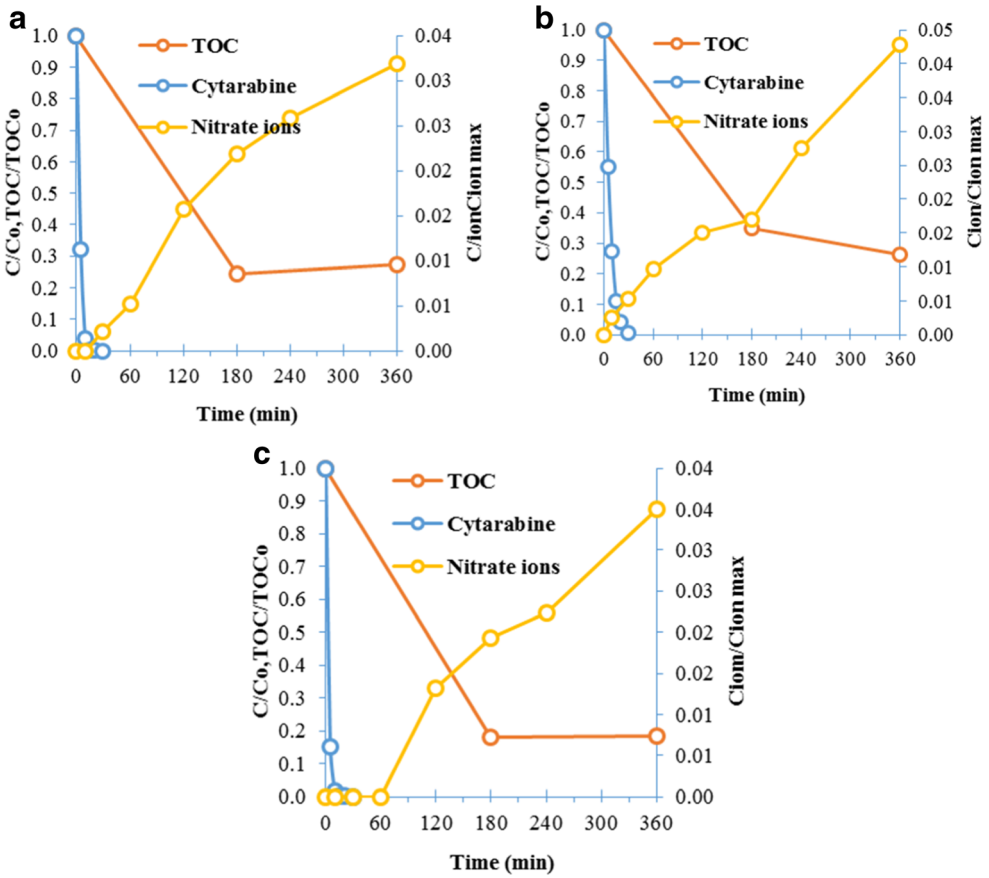

Fig. 3 Mineralization process of CY, SSL/Fe^{3+}/H_2O_2 (**a**); SSL/$Fe^{3+}/S_2O_8^{2-}$ (**b**); SSL/$[Fe(C_2O_4)_3]^{3-}/H_2O_2$, ($C_o$(CY) = 30 mg L^{-1}, $[Fe^{3+}]$ = 3 mg L^{-1}, [oxidant] = 90 mg L^{-1}) (**c**)

inhibiting the activation of the oxidant or they can act as scavengers of hydroxyl radicals (Kiwi et al. 2000, Pignatello 1992). Moreover, Bautitz and Nogueira (2010) (Bautitz and Nogueira 2010) attributed the higher efficiencies of the ferrioxalate to the higher quantum yield of Fe^{2+} production. Comparing the Fe^{3+}/H_2O_2/SSL system with $Fe^{3+}/S_2O_8^{2-}$/SSL, no great differences appear. However, the lower reaction rates achieved in the latter may be attributed to the slightly lower oxidation potential of sulfate radical and the different mechanisms taking place during the degradation (Wang et al. 2015). Moreover, previous studies proved that in transition metal–based activation reactions like Eqs. (4) and (13), iron is a better activator for peroxide than for persulfate (Anipsitakis and Dionysiou 2004).

Evaluation of TPs formed during photo-Fenton and photo-Fenton-like processes

The TPs generated during the photo-Fenton, photo-Fenton-like, and persulfate processes were identified through the analysis of mass spectra *m*/*z* ions, based on accurate mass measurements, as given by Table 1. Totally, twelve TPs were identified, four of which (TP 273, TP 277, TP 274 (I), and TP 274 (II)) were identified for the first time, to the best of our knowledge. Their proposed structures are depicted in Fig. 4. All of them were detected in low concentrations because of the very fast degradation kinetics that took place at all studied processes, and therefore their evolution profiles could not be obtained. The given

Table 1 High resolution mass spectra data for CY and identified TPs for the studied AOPs processes

t_R (min)	Code name	Pseudo-molecular ion formula	Theoretical *m*/*z* $[m+H]^+$	Experimental *m*/*z* $[m+H]^+$	Δ (ppm)	RDBE
1.51	CY	$C_9H_{14}N_3O_5$	244.0928	244.0922	2.4	4.5
		$C_4H_6N_3O$	112.0505	112.0506	−0.6	3.5
0.79	TP 111	$C_4H_6N_3O$	112.0505	112.0505	−0.3	3.5
		$C_4H_3N_2O$	95.0240	95.0233	−7.25	4.5
		$C_3H_5N_2$	69.0447	69.0441	−9.05	2.5
0.83	TP 291 (I)	$C_9H_{14}N_3O_8$	292.0775	292.0773	0.8	4.5
		$C_9H_{12}N_3O_7$	274.0670	274.0659	−3.9	5.5
		$C_8H_{11}N_2O_6$	231.0612	231.0601	−4.6	4.5
0.95	TP 259 (I)	$C_9H_{14}N_3O_6$	260.0877	260.0874	0.5	1.2
		$C_9H_{12}N_3O_5$	242.0771	242.0764	−3.08	5.5
		$C_4H_6N_3O$	112.0505	112.0500	−0.3	3.5
1.25	TP 259 (II)	$C_9H_{14}N_3O_6$	260.0877	260.0874	0.5	1.2
		$C_9H_{12}N_3O_5$	242.0771	242.0764	−3.08	5.5
		$C_4H_6N_3O$	112.0505	112.0500	−0.5	3.5
0.75	TP 275	$C_9H_{14}N_3O_7$	276.0826	276.0820	2.3	4.5
		$C_9H_{12}N_3O_6$	258.0721	258.0718	−1.0	5.5
		$C_4H_6N_3O$	112.0505	112.0502	−0.4	3.5
0.74	TP 291 (II)	$C_9H_{14}N_3O_8$	292.0775	292.0760	−1.5	4.5
		$C_9H_{12}N_3O_7$	274.0670	274.0659	−3.9	5.5
		$C_8H_{11}N_2O_6$	231.0612	231.0601	−4.6	4.5
0.83	TP 274 (I)*	$C_9H_{11}N_2O_8$	275.0510	275.0508	−0.7	5.5
0.87	TP 276 (I)	$C_9H_{13}N_2O_8$	277.0666	277.0662	−1.6	4.5
		$C_9H_{11}N_2O_7$	259.0561	259.0565		
0.91	TP 274 (II)*	$C_9H_{11}N_2O_8$	275.0510	275.0508	−0.7	5.5
		$C_9H_9N_2O_7$	257.0404	257.0406	−0.088	6.5
0.95	TP 276 (II)	$C_9H_{13}N_2O_8$	277.0666	277.0662	−1.6	4.5
		$C_9H_{11}N_2O_7$	259.0561	259.0560	−0.59	5.5
1.16	TP 273*	$C_9H_{12}N_3O_7$	274.0666	274.0667	−1.0	5.5
0.78	TP 277*	$C_9H_{16}N_3O_7$	278.0983	278.0979	−1.4	3.5
		$C_9H_{14}N_3O_6$	260.0877	260.0874	0.5	1.2
		$C_4H_6N_3O$	112.0505	112.0503	−2.1	3.5

*Identified for the first time in the present study

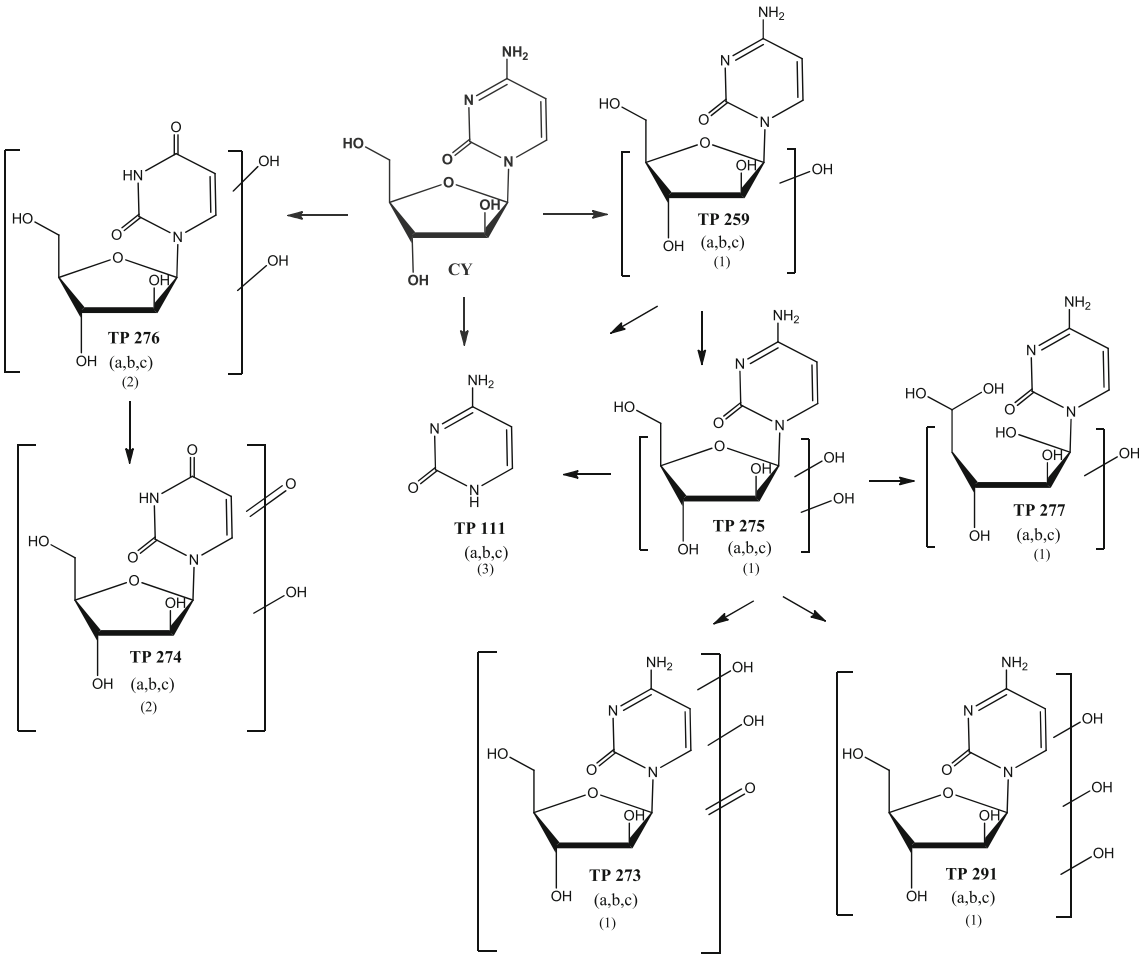

Fig. 4 Transformation of CY under SSL/Fe^{3+}/H_2O_2 (**a**), SSL/Fe^{3+}/$S_2O_8^{2-}$ (**b**), and SSL/$[Fe(C_2O_4)_3]^{3-}$/H_2O_2 (**c**) processes; transformation pathway 1 (1), transformation pathway 2 (2) and transformation pathway 3 (3)

generated TPs were identified during all the three studied processes. The MS^2 product ion spectra of major TPs of CY are given by Fig. S1. As reported also in a previous study of ours (Koltsakidou et al. 2017a), $HO^{\cdot}$ attack on CY molecule, resulting in the formation of hydroxylated TPs, TP 259 (I), and TP 259 (II). The presence of the fragment ion *m/z* 112.0505, that correspond to the pyrimidine ring of CY molecule, suggests that hydroxylation occurs at tetrahydrofuran ring (Fig. S1). Consecutive hydroxylation of CY molecule generated di- and tri-hydroxylated TPs (TP 275 and TP 291 (I, II)). The fragment ion at *m/z* 112.0505 was also observed for TP 275 fragmentation pattern, indicating again no hydroxylation at the pyrimidine ring of CY molecule (Fig. S1). The fragmentation of TP 291 indicates an initial loss of $–H_2O$ (*m/z* 274.0670) group, usual for hydroxylated TPs, and further loss of –CHNO group (*m/z* 231.0612), which corresponds to the cleavage of the pyrimidine ring (Fig. S1). TP 273 probably results from further oxidation of TP 275, which forms a keto-group. Furthermore, although that uracil arabinoside, formed from the breaking of C–NH_2 bond of CY molecule and subsequent oxidation of pyrimidine ring (Koltsakidou et al. 2017a), has not been detected in this study, hydroxylated uracil arabinoside TPs were detected (TP 276 I,II) during the applied processes. Their fragmentation data suggest loss of $–H_2O$ (*m/z* 259.0561). Further oxidation of TP 276 I, II, lead to the formation of keto-products, TP 274 I, II, where loss of $–H_2O$ (*m/z* 257.0404) was also observed during fragmentation. Additionally, one TP formed from the cleavage of tetrahydrofuran ring after subsequent oxidation-hydroxylation of CY molecule was identified (TP 277) and its fragmentation data (fragment ion *m/z* 112.0505) suggest that hydroxylation happened only at the tetrahydrofuran ring of CY molecule. Finally, TP 111 (cytosine) that corresponds to the pyrimidine ring of CY molecule was also detected as a CY breakdown product. As it has already been reported, TP 111 can lead to hydroxyl and de-aminated products (as also suggested by its fragmentation data, *m/z* 95.0240 corresponds to $–NH_3$ loss). These hydroxyl and de-aminated products may be finally transformed in tartronic, oxalic, mesoxalic, and lactic acid (Elsellami et al. 2014, Koltsakidou et al. 2017a).

Based on the structures found in this study and previously reported results in literature (Elsellami et al. 2014, Koltsakidou et al. 2017a), Fig. 4 summarizes the proposed transformation pathways by $HO^{\cdot}$ radical attack. Three different routes have been considered including hydroxylation that occurred preferably in the tetrahydrofuran ring of CY molecule with the subsequent oxidation (pathway 1), $HO^{\cdot}$ radical attack to aromatic ring and the substitution of NH_2 by HO group (pathway 2), and the cleavage of C–N bond (pathway 3).

Toxicity evaluation

Acute (LC50 and EC50) and chronic (ChV) toxicity of CY and its TPs were predicted using ECOSAR software. These kinds of predictions can be extremely helpful for water treatments, since the formation of potentially toxic TPs may be identified, enabling possible control (Tay and Madehi 2015). Acute and ChV toxicity levels were determined according to the Globally Harmonized System of Classification and Labelling of Chemicals, which is given by Table S1 (GHS 2011). The predicted ecotoxicity values of CY and its TPs on daphnia, fish, and green algae are categorized by the above classification and presented at Table 2. Each compound, depending on its chemical structure, may be classified by more than one toxicity class by ECOSAR program. Also, the predictions were contacted for more than one structure for some TPs (given at Electronic Supplementary Information (ESI)), since the exact hydroxylation and/or oxidation position cannot be determined accurately. The given structures are selected as the most representative for each compound, since ECOSAR calculations for possible other structures that are not given presented no difference, compared to those selected (Figs. S2–8).

According to the results, CY itself appears to present neither acute nor ChV toxicity on daphnia, fish, and green algae. As far as the CY-TPs is concerned, TP 274 and TP 276 may pose a threat, since they appear to have very toxic acute and chronic effect on green algae. Additionally, TP 274, TP 291, TP 276, TP 273 may present acute toxic effect and harmful or toxic chronic effect on daphnia. Furthermore, TP 274, TP 291, TP 276, and TP 273 are possibly a threat to fish, since according to the results, they present harmful both acute and chronic effect on them. Conclusively, the TPs generated during the studied AOP treatments appear to present aquatic toxicity, in contrast to the parent compound, that presents no toxicity at all. However, TP 273 (TP 273D) may be completely harmless, if the hydroxylation is conducted at the tetrahydrofuran ring and the pyrimidine amino group (Fig. S4). Also, TP 277 presents neither acute nor chronic toxicity. Additionally, there were no significant differences between the toxicity values obtained for TPs (TP 291, TP 273, TP 276), when the hydroxylation was conducted at different positions of pyrimidine or tetrahydrofuran ring of CY molecule (that belong at the same chemical class).

In our previous study, *Vibrio fischeri* bioassay was conducted, for CY and its degradation TPs by AOP treatment (Koltsakidou et al. 2017a). The initial CY solution presented very low toxicity (inhibition ~ 16%), while the TPs generated during the first minutes of the applied treatment presented increased toxicity (45% inhibition at 30 min of irradiation), which decreased later (5% inhibition after 180 min). All in all, the results obtained from *V. fischeri* bioassay are in accordance with the predictions conducted in silico in the present study, for CY and its TPs, since for most of the identified TPs, the predicted toxicity is higher than CY itself.

Application of the studied treatments for CY removal in wastewater matrix

The majority of studies related to the photocatalytic degradation of various organic pollutants are carried out in solutions of deionized or ultrapure water or simulated waste. In the present study, experiments of homogeneous photocatalytic degradation of CY were carried out in wastewater obtained from an effluent of a conventional wastewater treatment plant (WWTP). The wastewater effluent composition and physical characteristics are given at ESI (Table S2).

The experiments were carried out under the optimal conditions (Fig. S9). Since the resulting correlation coefficients were $R^2 > 0.95$, the first-order simplified model can be applied also to adequately describe the degradation of CY at complex wastewater matrix. The CY degradation rate constant, as well as the half-life (Table S3), is reduced in the sample from WWTP, compared to that obtained for ultrapure water, for all three studied treatments. This reduction can be attributed to the large amount of organic matter dissolved in the sample from WWTP (~ 12 mg L^{-1}), which consumes the oxidant species generated during the applied photocatalytic treatment (Jallouli et al. 2018). Also, the inorganic components, such as bicarbonates, chlorides, and sulfates, which are present in wastewaters act like scavengers of hydroxyl radicals, affecting the efficiency of the applied photocatalytic treatment (Shao et al. 2018).

Moreover, a higher consumption of the oxidant during the treatment of an effluent is expected since higher amount of TOC is treated and because chloride ions react also with peroxide through the reactions:

$$Cl^{\cdot} + H_2O_2 \rightarrow HO_2^{\cdot} + Cl^{-} + H^{+} \quad (17)$$

$$Cl_2^{\cdot -} + H_2O_2 \rightarrow HO_2^{\cdot} + 2Cl^{-} + H \quad (18)$$

However, all process can be considered effective since more than 60% degradation is achieved within 60 min of irradiation

Table 2 Predicted acute and chronic toxicity of CY and its TPs

	Acute toxicity (mg/L)			Chronic Toxicity (ChV) (mg/L)		
TPs (Chemical class)	**Fish (LC_{50})**	**Daphind (LC50)**	**Green Algae (EC50)**	**Fish**	**Daphind**	**Green Algae**
CY (AA)	39587	2811	6464	11183	139	1477
TP 111 (AA)	4047	322	590	805	17.9	147
TP 294 (V/A A)	117	7.89	5700000	1823	20.1	79306
TP 291 A (AA)	272000	16888	50664	116000	736	10508
TP 291 A (V/A A)	39.0	3.41	80954	57.5	2.01	2777
TP 291 B (AA)	41235	2959	6663	11274	148	1534
TP 291 B (V/A A)	25.4	2.46	15179	14.8	0.813	743
TP 291 C (V/A A)	30.0	2.80	29135	25.1	1.2	1242
TP 276 A (V/A A)	37.2	3.25	78436	55.5	1.93	2679
TP 276 A (CU)	46548	4030000	0.021	340	2983	0.006
TP 276 B (V/A A)	22.2	2.20	10456	10.8	0.649	548
TP 276 B(CU)	6770	127000	0.021	49.2	314	0.006
TP 259 A (AA)	16618	1267	2530	3774	67.4	609
TP 273 A (A)	12664	326000	141000	17071	16662	15110
TP 273 A (V/A A)	35.9	3.16	70456	50.8	1.81	2456
TP 273 B (A)	2500	32918	19367	1985	2169	2779
TP 273 B (AA)	30630	2238	4863	7929	114	1134
TP 273 B (V/A A)	22.6	2.22	11576	11.7	0.682	592
TP 273 C (A)	31712	1190000	436000	57684	52820	39390
TP 273 C (AA)	742000	42435	150000	405000	405000	29274
TP 273 C (V/A A)	46.6	3.85	196000	116	3.15	5492
TP 273 D (A)	998	8993	6286	587	684	1066
TP 275	10208	812	1491	2039	45.0	370
TP 277	801000	45593	162000	444000	1825	31641
TP 274 A (CU)	51843	4920000	0.021	379	3387	0.006
TP 274 A (A)	15439	431000	180000	22178	21355	18580
TP 274 A (V/A A)	38.1	3.31	87814	60.8	2.04	2923
TP 274 B (A)	1217	11883	8008	763	877	1311
TP 274 B (V/A A)	18.4	1.90	5193	6.12	0.443	315
TP 274 B(CU)	3464	38342	0.021	25.1	144	0.006
TP 274 C(CU)	5385	13585	0.206	38.8	163	0.056

ECOSAR classification: *NO* neutral organics, *V/A A* vinyl/allyl alcohols, *CU* carbonyl ureas, *AA* aliphatic amines, *A* aldehydes Very toxic | Toxic | Harmful | Not harmful

time while with the ferrioxalate system, 85% degradation is observed. Prolonged irradiation times and higher initial doses of iron and hydrogen peroxide that are commonly used in the treatment of effluents of WWTPs would give a higher removal outcome (Bautitz and Nogueira 2010, Gómez et al. 2008).

Conclusions

The investigation of CY degradation by photo-Fenton (Fe^{3+}/H_2O_2/SSL) and photo-Fenton-like treatments (Fe^{3+}/$S_2O_8^{2-}$/SSL and $[Fe(C_2O_4)_3]^{3-}$/H_2O_2/SSL) was conducted in this study. Under optimized conditions, CY's complete removal was achieved in less than 45 min, by all treatments applied. The conducted mineralization studies indicated that $[Fe(C_2O_4)_3]^{3-}$/H_2O_2/SSL treatment was the most efficient, since TOC reduction reached 82% after 360 min of SSL irradiation, compared to 73% TOC reduction achieved by Fe^{3+}/H_2O_2/SSL and Fe^{3+}/$S_2O_8^{2-}$/SSL treatments, at the same irradiation time. In addition, twelve TPs were identified during the applied processes, four of which were identified for the first time. Their identification was conducted by liquid chromatography coupled to high resolution mass spectrometry. According to suggested structures of the generated TPs, CY's transformation during the applied treatments occurred mainly by hydroxylation and subsequent oxidation. Last but not least, the predicted values of acute and chronic toxicity for CY and its TPs on fish, daphnia, and green algae suggested that the TPs generated during the studied AOP treatments may pose a threat to aquatic environment, in contrast to the parent compound that presents negligible toxicity. Finally, all the applied techniques presented lower degradation efficiencies when used in wastewater matrix, compared to those obtained for ultrapure water due to the presence of organic matter and inorganic ions acting as radical scavengers.

Acknowledgments The authors would like to thank the Unit of LC-MS/MS of the Aristotle University of Thessaloniki for providing access in the facilities.

Funding information This research has been co-financed—via a program of State Scholarships Foundation (IKY)—by the European Union (European Social Fund—ESF) and Greek national funds through the action entitled "Strengthening Human Resources Research Potential via Doctorate Research" in the framework of the operational program "Human Resources Development Program, Education and Lifelong Learning" of the National Strategic Reference Framework (NSRF) 2014–2020.

Compliance with ethical standards

Conflict of interest The authors declare that they have no conflict of interest.

References

Abdessalem AK, Oturan N, Bellakhal N, Dachraoui M, Oturan MA (2008) Experimental design methodology applied to electro-Fenton treatment for degradation of herbicide chlortoluron. Appl Catal B Environ 78:334–341

Anipsitakis GP, Dionysiou DD (2004) Transition metal/UV-based advanced oxidation technologies for water decontamination. Appl Catal B Environ 54:155–163

Antonopoulou M, Giannakas A, Deligiannakis Y, Konstantinou I (2013) Kinetic and mechanistic investigation of photocatalytic degradation of the N,N-diethyl-m-toluamide. Chem Eng J 231:314–325

Avetta P, Pensato A, Minella M, Malandrino M, Maurino V, Minero C, Hanna K, Vione D (2015) Activation of persulfate by irradiated magnetite: implications for the degradation of phenol under heterogeneous photo-fenton-like conditions. Environ Sci Technol 49:1043–1050

Bautitz IR, Nogueira RFP (2010) Photodegradation of lincomycin and diazepam in sewage treatment plant effluent by photo-Fenton process. Catal Today 151:94–99

Dal Bosco SM, Barbosa IM, Candello FP, Maniero MG, Rath S, Guimarães JR (2011) Degradation of ivermectin by Fenton and photo-Fenton and toxicity test using Daphnia similis. J Adv Oxid Technol 14:292–301

Ding D, Liu C, Ji Y, Yang Q, Chen L, Jiang C, Cai T (2017) Mechanism insight of degradation of norfloxacin by magnetite nanoparticles activated persulfate: identification of radicals and degradation pathway. Chem Eng J 308:330–339

Dong H, Zeng G, Tang L, Fan C, Zhang C, He X, He Y (2015) An overview on limitations of TiO_2-based particles for photocatalytic degradation of organic pollutants and the corresponding countermeasures. Water Res 79:128–146

Doumic LI, Soares PA, Ayude MA, Cassanello M, Boaventura RAR, Vilar VJP (2015) Enhancement of a solar photo-Fenton reaction by using ferrioxalate complexes for the treatment of a synthetic cotton-textile dyeing wastewater. Chem Eng J 277:86–96

Elsellami L, Sahel K, Dappozze F, Horikoshi S, Houas A, Guillard C (2014) Titania-based photocatalytic degradation of two nucleotide bases, cytosine and uracil. Appl Catal A Gen 485:207–213

Evgenidou E, Konstantinou I, Fytianos K, Poulios I (2007) Oxidation of two organophosphorous insecticides by the photo-assisted Fenton reaction. Water Res 41:2015–2027

Ferri P, Ramil M, Rodríguez I, Bergamasco R, Vieira AMS, Cela R (2017) Assessment of quinoxyfen phototransformation pathways by liquid chromatography coupled to accurate mass spectrometry. Anal Bioanal Chem 409:2981–2991

Gao H, Chen J, Zhang Y, Zhou X (2016) Sulfate radicals induced degradation of Triclosan in thermally activated persulfate system. Chem Eng J 306:522–530

Gar Alalm M, Tawfik A, Ookawara S (2015) Comparison of solar TiO_2 photocatalysis and solar photo-Fenton for treatment of pesticides industry wastewater: operational conditions, kinetics, and costs. J Water Proc Eng 8:55–63

GHS (2011) In: Nations U (ed) (Hrsg.), 4th edGlobally harmonized system of classification and labelling of chemical (GHS). United Nations Publications, New York

Gómez MJ, Sirtori C, Mezcua M, Fernández-Alba AR, Agüera A (2008) Photodegradation study of three dipyrone metabolites in various water systems: identification and toxicity of their photodegradation products. Water Res 42:2698–2706

Hu J-Y, Tian K, Jiang H (2016) Improvement of phenol photodegradation efficiency by a combined g-C3N4/Fe(III)/persulfate system. Chemosphere 148:34–40

Irmak S, Kusvuran E, Erbatur O (2004) Degradation of 4-chloro-2-methylphenol in aqueous solution by UV irradiation in the presence of titanium dioxide. Appl Catal B Environ 54:85–91

Isidori M, Lavorgna M, Russo C, Kundi M, Žegura B, Novak M, Filipič M, Mišík M, Knasmueller S, de Alda ML, Barceló D, Žonja B, Česen M, Ščančar J, Kosjek T, Heath E (2016a) Chemical and toxicological characterisation of anticancer drugs in hospital and municipal wastewaters from Slovenia and Spain. Environ Pollut 219: 275–287

Isidori M, Piscitelli C, Russo C, Smutná M, Bláha L (2016b) Teratogenic effects of five anticancer drugs on Xenopus laevis embryos. Ecotoxicol Environ Saf 133:90–96

Ismail L, Ferronato C, Fine L, Jaber F, Chovelon J-M (2017) Elimination of sulfaclozine from water with $SO_4^{\cdot-}$ radicals: evaluation of different persulfate activation methods. Appl Catal B Environ 201:573–581

Jallouli N, Pastrana-Martínez LM, Ribeiro AR, Moreira NFF, Faria JL, Hentati O, Silva AMT, Ksibi M (2018) Heterogeneous photocatalytic degradation of ibuprofen in ultrapure water, municipal and pharmaceutical industry wastewaters using a TiO2/UV-LED system. Chem Eng J 334:976–984

Kamińska B, Majewska K, Skwierawska A, Kozłowska-Tylingo K (2018) Degradation kinetics and mechanism of pentoxifylline by ultraviolet activated peroxydisulfate. RSC Adv 8:23648–23656

Katheresan V, Kansedo J, Lau SY (2018) Efficiency of various recent wastewater dye removal methods: a review. J Environ Chem Eng 6: 4676–4697

Kiwi J, Lopez A, Nadtochenko V (2000) Mechanism and kinetics of the OH-radical intervention during fenton oxidation in the presence of a significant amount of radical scavenger (Cl−). Environ Sci Technol 34:2162–2168

Koltsakidou A, Antonopoulou M, Evgenidou E, Konstantinou I, Lambropoulou DA (2017a) Cytarabine degradation by simulated solar assisted photocatalysis using TiO_2. Chem Eng J 316:823–831

Koltsakidou A, Antonopoulou M, Sykiotou M, Evgenidou E, Konstantinou I, Lambropoulou DA (2017b) Photo-Fenton and Fenton-like processes for the treatment of the antineoplastic drug 5-fluorouracil under simulated solar radiation. Environ Sci Pollut Res 24:4791–4800

Koltsakidou A, Antonopoulou M, Evgenidou E, Konstantinou I, Giannakas AE, Papadaki M, Bikiaris D, Lambropoulou DA (2017c) Photocatalytical removal of fluorouracil using TiO_2-P25 and N/S doped TiO_2 catalysts: a kinetic and mechanistic study. Sci Total Environ 578:257–267

Kosjek T, Heath E (2011) Occurrence, fate and determination of cytostatic pharmaceuticals in the environment. TrAC Trends Anal Chem 30: 1065–1087

Lambropoulou D, Evgenidou E, Saliverou V, Kosma C, Konstantinou I (2017) Degradation of venlafaxine using TiO_2/UV process: kinetic studies, RSM optimization, identification of transformation products and toxicity evaluation. J Hazard Mater 323:513–526

Li B, Dong Y, Wang P, Cui G (2015) Ferrioxalate-assisted solar photo-Fenton degradation of reactive dyes in the presence of inorganic salts. Fibers Polym 16:2325–2336

Lin HH-H, Lin AY-C (2014) Photocatalytic oxidation of 5-fluorouracil and cyclophosphamide via UV/TiO_2 in an aqueous environment. Water Res 48:559–568

Liu J, Jiang Y, Cui Y, Xu C, Ji X, Luan Y (2014) Cytarabine-AOT catanionic vesicle-loaded biodegradable thermosensitive hydrogel as an efficient cytarabine delivery system. Int J Pharm 473:560–571

Lucas MS, Peres JA (2007) Degradation of reactive Black 5 by Fenton/UV-C and ferrioxalate/H_2O_2/solar light processes. Dyes Pigments 74:622–629

Lutterbeck CA, Baginska E, Machado ÊL, Kümmerer K (2015a) Removal of the anti-cancer drug methotrexate from water by advanced oxidation processes: aerobic biodegradation and toxicity studies after treatment. Chemosphere 141:290–296

Lutterbeck CA, Machado ÊL, Kümmerer K (2015b) Photodegradation of the antineoplastic cyclophosphamide: a comparative study of the efficiencies of UV/H_2O_2, UV/Fe_2+/H_2O_2 and UV/TiO_2 processes. Chemosphere 120:538–546

Martín J, Camacho-Muñoz D, Santos JL, Aparicio I, Alonso E (2011) Simultaneous determination of a selected group of cytostatic drugs in water using high-performance liquid chromatography–triple-quadrupole mass spectrometry. J Sep Sci 34:3166–3177

Martínez-Costa JI, Rivera-Utrilla J, Leyva-Ramos R, Sánchez-Polo M, Velo-Gala I, Mota AJ (2018) Individual and simultaneous degradation of the antibiotics sulfamethoxazole and trimethoprim in aqueous solutions by Fenton, Fenton-like and photo-Fenton processes using solar and UV radiations. J Photochem Photobiol A Chem 360:95–108

Matta R, Tlili S, Chiron S, Barbati S (2011) Removal of carbamazepine from urban wastewater by sulfate radical oxidation. Environ Chem Lett 9:347–353

Méndez-Arriaga F, Esplugas S, Giménez J (2010) Degradation of the emerging contaminant ibuprofen in water by photo-Fenton. Water Res 44:589–595

Michael I, Hapeshi E, Michael C, Fatta-Kassinos D (2010) Solar Fenton and solar TiO_2 catalytic treatment of ofloxacin in secondary treated effluents: evaluation of operational and kinetic parameters. Water Res 44:5450–5462

Monteagudo JM, Durán A, Aguirre M, Martín IS (2010) Photodegradation of reactive blue 4 solutions under ferrioxalate-assisted UV/solar photo-Fenton system with continuous addition of H_2O_2 and air injection. Chem Eng J 162:702–709

Ocampo-Pérez R, Sánchez-Polo M, Rivera-Utrilla J, Leyva-Ramos R (2010) Degradation of antineoplastic cytarabine in aqueous phase by advanced oxidation processes based on ultraviolet radiation. Chem Eng J 165:581–588

Ocampo-Pérez R, Sánchez-Polo M, Rivera-Utrilla J, Leyva-Ramos R (2011) Enhancement of the catalytic activity of TiO_2 by using activated carbon in the photocatalytic degradation of cytarabine. Appl Catal B Environ 104:177–184

Ocampo-Pérez R, Rivera-Utrilla J, Mota AJ, Sánchez-Polo M, Leyva-Ramos R (2016) Effect of radical peroxide promoters on the photodegradation of cytarabine antineoplastic in water. Chem Eng J 284:995–1002

Pignatello JJ (1992) Dark and photoassisted iron(3+)-catalyzed degradation of chlorophenoxy herbicides by hydrogen peroxide. Environ Sci Technol 26:944–951

Pignatello JJ, Oliveros E, MacKay A (2006) Advanced oxidation processes for organic contaminant destruction based on the Fenton reaction and related chemistry. Crit Rev Environ Sci Technol 36:1–84

Raies AB, Bajic VB (2016) In silico toxicology: computational methods for the prediction of chemical toxicity. Wiley Interdisciplinary Reviews. Comput Mol Sci 6:147–172

Ribeiro AR, Nunes OC, Pereira MFR, Silva AMT (2015) An overview on the advanced oxidation processes applied for the treatment of water pollutants defined in the recently launched Directive 2013/39/EU. Environ Int 75:33–51

Shao H-y, Wu M-h, Deng F, Xu G, Liu N, Li X, Tang L (2018) Electron beam irradiation induced degradation of antidepressant drug fluoxetine in water matrices. Chemosphere 190:184–190

Soltani T, Lee B-K (2017) Enhanced formation of sulfate radicals by metal-doped $BiFeO_3$ under visible light for improving photo-Fenton catalytic degradation of 2-chlorophenol. Chem Eng J 313: 1258–1268

Soltermann F, Abegglen C, Tschui M, Stahel S, von Gunten U (2017) Options and limitations for bromate control during ozonation of wastewater. Water Res 116:76–85

Tamimi M, Qourzal S, Barka N, Assabbane A, Ait-Ichou Y (2008) Methomyl degradation in aqueous solutions by Fenton's reagent and the photo-Fenton system. Sep Purif Technol 61:103–108

Tay KS, Madehi N (2015) Ozonation of ofloxacin in water: by-products, degradation pathway and ecotoxicity assessment. Sci Total Environ 520:23–31

Toolaram AP, Kümmerer K, Schneider M (2014) Environmental risk assessment of anti-cancer drugs and their transformation products: a focus on their genotoxicity characterization-state of knowledge and short comings. Mutat Res Rev Mutat Res 760:18–35

Wang Y, Liu H, Liu G, Xie Y, Gao S (2015) Oxidation of diclofenac by potassium ferrate (VI): reaction kinetics and toxicity evaluation. Sci Total Environ 506-507:252–258

Zhang J, Chang VWC, Giannis A, Wang J-Y (2013) Removal of cytostatic drugs from aquatic environment: a review. Sci Total Environ 445–446:281–298